Monitoring PSR B1509–58 with *RXTE*: Spectral analysis 1996–2010

E. Litzinger, K. Pottschmidt, J. Wilms, S. Suchy, R. E. Rothschild, I. Kreykenbohm

Abstract

We present an analysis of the X-ray spectra of the young, Crab-like pulsar PSR B1509–58 (pulse period $P \sim 151\,\mathrm{ms}$) observed by *RXTE* over 14 years since the beginning of the mission in 1996. The uniform dataset is especially well suited for studying the stability of the spectral parameters over time as well as for determining pulse phase resolved spectral parameters with high significance. The phase averaged spectra as well as the resolved spectra can be well described by an absorbed power law.

Keywords: pulsars: individual (PSR B1509–58) — stars: neutron — X-rays: stars.

1 Introduction

The pulsar PSR B1509–58 was discovered in *Einstein X-Ray Observatory* data from 1979 and 1980 [5]. The pulsar is associated with the supernova remnant G320.4–1.2 (MSH 15–52) in the constellation Circinus.

PSR B1509–58 has been established as one of only a few known Crab-like sources, i.e., a young pulsar powering a synchrotron nebula [6]. PSR B1509–58's nebula is considerably larger, its surface brightness is lower and the pulse period of $P \sim 151\,\mathrm{ms}$ is slower than that of the Crab. Due to a very high spin-down rate of $\dot{P} \sim 1.5 \times 10^{-12}\,\mathrm{s\ s^{-1}}$, however, the characteristic age $P/2\dot{P}$ of PSR B1509–58 is $\sim 1.6 \times 10^3\,\mathrm{yr}$ (e.g., [7]), i.e., comparable to that of the Crab ($\sim 1.3 \times 10^3\,\mathrm{yr}$).

In the following we analyse the phase averaged spectra (Sec. 2) and the phase resolved spectra (Sec. 5) from calculated ephemerides (Sec. 3) for the three major calibration epochs 3–5 for the *RXTE*. Pulse profiles for the epochs are presented in Sec. 4. A short summary of the results and the implications for further spectral analysis with *RXTE* are given in Sec. 6

2 Phase averaged spectra

From approximately monthly monitoring observations of PSR B1509–58 time averaged PCA (PCU2 top layer, [1, 2]) and HEXTE (cluster A and B, [4]) spectra were created by averaging individual monitoring spectra over major instrument calibration epochs, i.e. between MJD 50188 and 51259 (epoch 3), MJD 51259 and 51677 (epoch 4), and from MJD 51677 onward (epoch 5). Figure 1 shows the epoch averaged counts spectra for epoch 5. Some spectral parameters and their uncertainties for the three fits are given in Table 1. No systematic uncertainties have been added to the spectra.

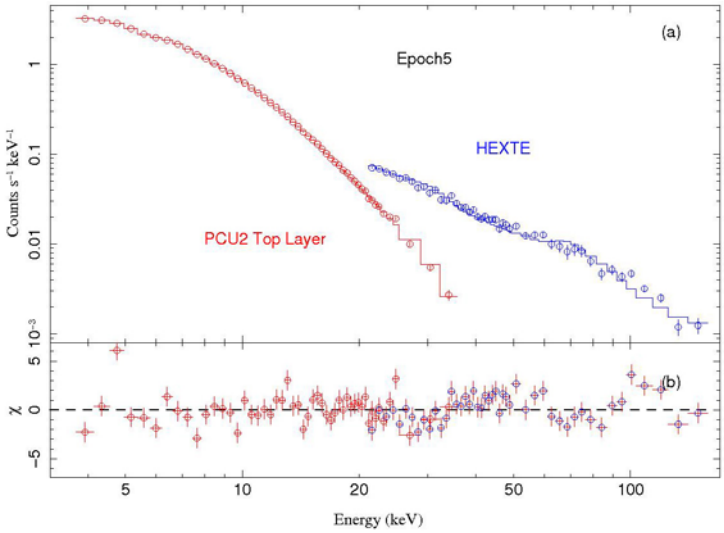

Fig. 1: (a) PCU2 top layer and HEXTE counts spectra obtained by accumulating all suitable monitoring spectra of epoch 5 and best simultaneous fit model (absorbed power law with an iron line), (b) Best fit residuals

Table 1: Best fit parameters for the phase averaged PCU2 spectra of calibration epoch 3–5

Parameter	Epoch 3	Epoch 4	Epoch 5
Γ	2.022 ± 0.001	2.021 ± 0.001	2.026 ± 0.001
A_Γ $\left[10^{-2}\,\mathrm{keV}^{-1}\,\mathrm{cm}^{-2}\,\mathrm{s}^{-1}\right]$	7.48 ± 0.84	7.48 ± 1.01	7.33 ± 0.12
N_H $\left[10^{22}\,\mathrm{cm}^{-2}\right]$	0.37 ± 0.01	0.39 ± 0.02	0.58 ± 0.02
E_Fe [keV]	$6.65^{+0.01}_{-0.16}$	$6.50^{+0.16}_{-0.03}$	6.50 ± 0.03
c_HEXTE	0.65 ± 0.05	0.76 ± 0.04	0.85 ± 0.02
$\chi^2_\mathrm{red}/\mathrm{dof}$	1.09/48	0.58/42	2.16/94
$F_{4-10\,\mathrm{keV}}$ $\left[10^{-11}\,\mathrm{erg\,cm^{-2}s^{-1}}\right]$	10.25	10.34	9.85
$F^\mathrm{unabs}_{4-10\,\mathrm{keV}}$ $\left[10^{-11}\,\mathrm{erg\,cm^{-2}s^{-1}}\right]$	10.57	10.57	9.93
$F_{10-20\,\mathrm{keV}}$ $\left[10^{-11}\,\mathrm{erg\,cm^{-2}s^{-1}}\right]$	7.76	7.76	7.20
$F_{20-200\,\mathrm{keV}}$ $\left[10^{-11}\,\mathrm{erg\,cm^{-2}s^{-1}}\right]$	25.07	25.15	22.36

The spectra are modeled by an absorbed power law. In addition we found clear indications of a narrow iron Kα line which is included by a Gaussian component added to the power law. Because of the long monitoring time of epoch 5 (ten years) systematic features are visible in the spectra. For the PCA there are strong residuals around 5 keV depending on the three xenon L edges. Around 9.3 keV a broad negative residual is visible. We model it with an additional negative Gaussian line at this energy with a flux of $-3 \times 10^{-5}\,\mathrm{cm}^{-2}\,\mathrm{s}^{-1}$. We speculate that this residual might be related to imperfect modeling of the copper Kα emission line at 8.04 keV. Also events from the americium calibration source of the PCA at 33 keV are visible. They were also modeled with a negative Gaussian line with a flux of $-1.4 \times 10^{-4}\,\mathrm{cm}^{-2}\,\mathrm{s}^{-1}$.

3 Pulse period ephemeris

The pulse phase resolved analysis for the PCA is based on high time-resolution `GoodXenon` event mode data, filtered for PCU2 top layer events. Ephemerides for PSR B1509–58 were calculated from the pulse frequencies of each observation. The reference epoch was set to $t_0(\mathrm{MJD}) = 52\,921.0$, the averaged time of the monitoring (see Figure 2, Table 2). With this result barycentered pulse phase- and energy resolved source count rates (`pha2` files) were created using a modified version of the `FTOOL` *fasebin* [3].

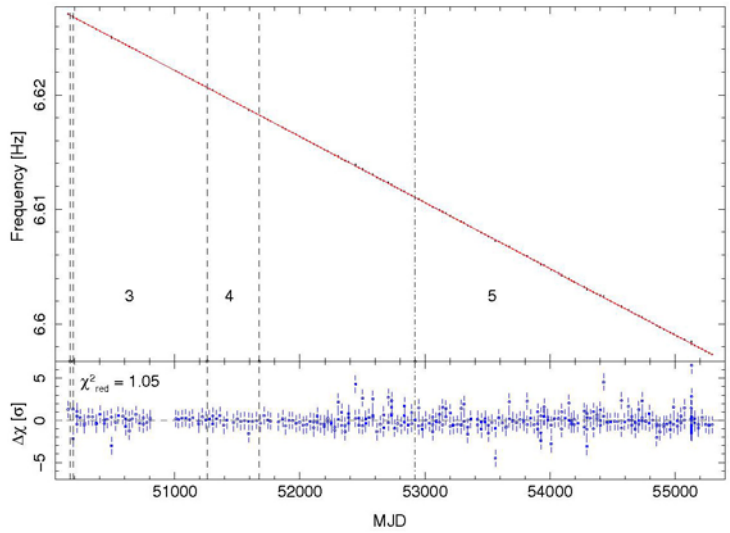

Fig. 2: Frequencies of each observation, calculated by epoch folding the barycentered `GoodXenon` lightcurve, vs. time with the best fit of a polynomial of quartic grade. A linear decline is visible

Table 2: Values for the pulse frequency and its first three derivatives

$\nu\ \left[\mathrm{s}^{-1}\right]$	$\dot{\nu}\ \left[10^{-11}\,\mathrm{s}^{-2}\right]$	$\ddot{\nu}\ \left[10^{-21}\,\mathrm{s}^{-3}\right]$	$\dddot{\nu}\ \left[10^{-29}\,\mathrm{s}^{-4}\right]$
$6.610\,32 \pm 1\mathrm{e}-6$	$-6.696\,5 \pm 0.002$	1.18 ± 0.24	1.77 ± 0.36

4 Pulse profiles

Pulse profiles in the energy range 3–43 keV for the three major epochs are shown in Figure 3. The peak was centered to phase 1.0 by shifting the individual pulse profiles and adding them up. The decline in rate between epochs is an instrumental effect and is accounted for in the calibration of the PCU2 top layer. The bigger errorbars in epoch 4 are due to a shorter duration and therefore less observations (30 in epoch 3, 13 in epoch 4, 213 in epoch 5). A clear division in peak $\Phi = 0.88 - 1.25$ and off-peak $\Phi = 0.44 - 0.75$ is possible.

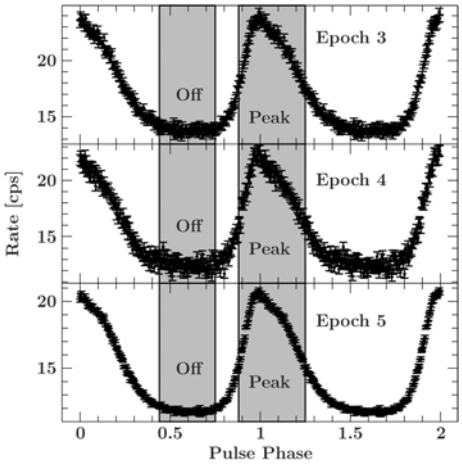

Fig. 3: Pulse profiles for the energy range 3–43 keV of PSR B1509–58 for the three major epochs 3, 4 and 5

5 Phase resolved spectra

All pulsed (i.e., peak minus off-peak) and unpulsed (regular background) spectra were summed to obtain averaged spectra for epochs 3–5, respectively. For the averaged phase resolved spectra, as for the phase averaged spectra before, an absorbed power law was fitted (energy range 3–20 keV). For epoch 5 it showed that the residuals for the pulsed emission improved by including a cutoff (see Figures 4 and 5). The pulsed spectra showed no indication for an iron line at 6.4 keV. The line is part of the unpulsed spectra and hence of the PWN of PSR B1509–58. This is also the explanation for the different values of the N_{H}. In the pulsed emission we see the beam of the pulsar and the galactic extinction. In the unpulsed emission we see the surrounding PWN without the pulsar and the galactic extinction. Therefore the value for the latter is smaller than for the pulsed emission. The best fit parameters for epoch 5 are shown in Table 3.

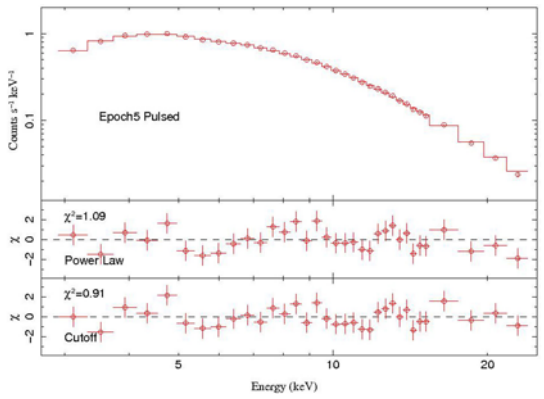

Fig. 4: PCU2 top layer counts spectra of the pulsed emission of epoch 5. Residuals are shown for an absorbed power law and after including a cutoff

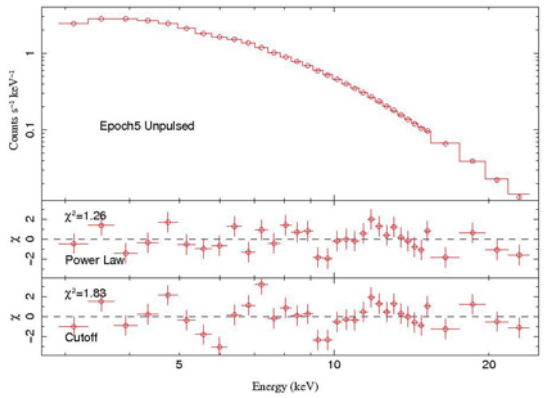

Fig. 5: The same as Figure 4 but for the unpulsed emission

Table 3: Best fit parameters for the pulsed and unpulsed emission for epoch 5

Parameter	E5 pulsed	E5 pulsed	E5 unpulsed
Γ	1.37 ± 0.01	1.27 ± 0.01	2.27 ± 0.01
E_{cut} [keV]		116 ± 8	
N_{H} $\left[10^{22}\mathrm{cm}^{-2}\right]$	2.40 ± 0.1	1.97 ± 0.11	1.34 ± 0.02
E_{Fe} [keV]			$6.57^{+0.01}_{-0.07}$
$F_{4-10\,\mathrm{keV}}$ $\left[10^{-11}\,\mathrm{erg\,cm}^{-2}\mathrm{s}^{-1}\right]$	4.28 ± 0.02	4.29 ± 0.02	7.99 ± 0.01
$F^{\mathrm{unabs}}_{4-10\,\mathrm{keV}}$ $\left[10^{-11}\,\mathrm{erg\,cm}^{-2}\mathrm{s}^{-1}\right]$	4.57 ± 0.02	4.52 ± 0.02	8.30 ± 0.01
$F_{10-20\,\mathrm{keV}}$ $\left[10^{-11}\,\mathrm{erg\,cm}^{-2}\mathrm{s}^{-1}\right]$	5.56 ± 0.02	5.57 ± 0.02	4.90 ± 0.01
χ^2_{red}	1.09	0.91	1.26

6 Summary and conclusions

We could well describe the spectra with an absorbed power law with a Gaussian line for the phase averaged and the unpulsed spectra and without the Gaussian for the pulsed spectra. For the pulsed spectrum of epoch 5 a cutoff improves the fit, while for the other epochs and the unpulsed emission it has no effect. No significant changes between the values of the different epochs for the averaged, pulsed and unpulsed emission were seen. Long observations show systematic effects from the instruments and are therefore good for describing the calibration effects. As forthcoming work we intend to add HEXTE spectra to the epoch averaged phase resolved analysis.

References

[1] Jahoda, K., Swank, J. H., Giles, A. B., et al.: *Proc. EUV, X-Ray, and Gamma-Ray Instrumentation for Astronomy VII*, 1996, Vol. **2 808**, 59.

[2] Jahoda, K., Markwardt, C. B., Radeva, Y., et al.: *ApJS*, 163, **401**, 2006.

[3] Kreykenbohm, I., Coburn, W., Wilms, J., et al.: A&A 395, **129**, 2002.

[4] Rothschild, R. E., Blanco, P. R., Gruber, D. E., et al.: *ApJ*, 496, **538**, 1998.

[5] Seward, F. D., Harnden, Jr. F. R.: *ApJ*, 256, **L45**, 1982.

[6] Seward, F. D., Harnden, Jr. F. R., Szymkowiak, A., et al.: *ApJ*, 281, **650**, 1984.

[7] Zhang, L., Cheng, K. S.: *A&A*, 363, **575**, 2000.

E. Litzinger
Dr. Remeis-Observatory/ECAP, FAU
Bamberg, Germany

K. Pottschmidt
CRESST/NASA-GSFC
Greenbelt, MD, USA
UMBC
Baltimore, MD, USA

J. Wilms
Dr. Remeis-Observatory/ECAP, FAU
Bamberg, Germany

S. Suchy
CASS/UCSD
La Jolla, CA, USA

R. E. Rothschild
CASS/UCSD
La Jolla, CA, USA

I. Kreykenbohm
Dr. Remeis-Observatory/ECAP, FAU
Bamberg, Germany